
Princeton Plasma Physics Laboratory

PPPL-

PPPL-



Prepared for the U.S. Department of Energy under Contract DE-AC02-76CH03073.

Princeton Plasma Physics Laboratory

Report Disclaimers

Full Legal Disclaimer

This report was prepared as an account of work sponsored by an agency of the United States Government. Neither the United States Government nor any agency thereof, nor any of their employees, nor any of their contractors, subcontractors or their employees, makes any warranty, express or implied, or assumes any legal liability or responsibility for the accuracy, completeness, or any third party's use or the results of such use of any information, apparatus, product, or process disclosed, or represents that its use would not infringe privately owned rights. Reference herein to any specific commercial product, process, or service by trade name, trademark, manufacturer, or otherwise, does not necessarily constitute or imply its endorsement, recommendation, or favoring by the United States Government or any agency thereof or its contractors or subcontractors. The views and opinions of authors expressed herein do not necessarily state or reflect those of the United States Government or any agency thereof.

Trademark Disclaimer

Reference herein to any specific commercial product, process, or service by trade name, trademark, manufacturer, or otherwise, does not necessarily constitute or imply its endorsement, recommendation, or favoring by the United States Government or any agency thereof or its contractors or subcontractors.

PPPL Report Availability

Princeton Plasma Physics Laboratory:

<http://www.pppl.gov/techreports.cfm>

Office of Scientific and Technical Information (OSTI):

<http://www.osti.gov/bridge>

Related Links:

[U.S. Department of Energy](#)

[Office of Scientific and Technical Information](#)

[Fusion Links](#)

Momentum Transport in Electron-Dominated Spherical Torus Plasmas

S.M. Kaye 1), W. Solomon 1), R. E. Bell 1), B.P. LeBlanc 1), F. Levinton 2), J. Menard 1), G. Rewoldt 1), S. Sabbagh 3), W. Wang 1), H. Yuh 2)

1) Princeton Plasma Physics Laboratory, Princeton University, Princeton, NJ 08543

2) Nova Photonics, Princeton, NJ 08543

3) Dept. of Applied Physics, Columbia University, NY, NY 10027

email contact of main author: skaye@pppl.gov

Abstract. The National Spherical Torus Experiment (NSTX) operates between 0.35 and 0.55 T, which, when coupled to up to 7 MW of neutral beam injection, leads to central rotation velocities in excess of 300 km/s and ExB shearing rates up to 1 MHz. This level of ExB shear can be up to a factor of five greater than typical linear growth rates of long-wavelength ion (e.g., ITG) modes, at least partially suppressing these instabilities. Evidence for this turbulence suppression is that the inferred diffusive ion thermal flux in NSTX H-modes is often at the neoclassical level, and thus these plasmas operate in an electron-dominated transport regime. Analysis of experiments using $n=3$ magnetic fields to change plasma rotation indicate that local rotation shear influences local transport coefficients, most notably the ion thermal diffusivity, in a manner consistent with suppression of the low- k turbulence by this rotation shear. The value of the effective momentum diffusivity, as inferred from steady-state momentum balance, is found to be larger than the neoclassical value. Results of perturbative experiments indicate inward pinch velocities up to 40 m/s and perturbative momentum diffusivities of up to 4 m^2/s , which are larger by a factor of several than those values inferred from steady-state analysis. The inferred pinch velocity values are consistent with values based on theories in which low- k turbulence drives the inward momentum pinch. Thus, in Spherical Tori (STs), while the neoclassical ion energy transport effects can be relatively high and dominate the ion energy transport, the neoclassical momentum transport effects are near zero, meaning that transport of momentum is dominated by any low- k turbulence that exists.

1. Introduction

Plasma rotation in magnetic confinement devices plays a critical role for optimizing fusion plasma performance through shear stabilization of both the microturbulence that is associated with heat and energy transport as well as macroscopic magnetohydrodynamic (MHD) instabilities. In particular, ExB shear is believed to play a role in stabilizing both low- k turbulence from Ion Temperature Gradient (ITG) and Trapped Electron Modes (TEM) [1-3], and has recently been associated with a suppression of high- k turbulence from Electron Temperature Gradient (ETG) modes [4]. Additionally, ExB shearing has been noted to suppress both internal MHD modes [5] as well as external, Resistive Wall Modes (RWM) [6, 7]. It has been only recently that studies of the sources of plasma rotation and momentum transport have been performed, and, therefore, the understanding of the underlying physics of these is still developing. Understanding the source of the momentum transport, and how it scales to larger devices operating at lower collisionality, is critical to the performance of future Spherical Torus (ST)-based Fusion Energy Development devices such as an ST-based Component Test Facility, as well as to conventional aspect ratio devices such as ITER, which is also expected to operate in electron-dominated transport regimes.

The Spherical Torus, or low aspect ratio tokamak, characteristically operates at sub-Tesla toroidal fields, leading to high ExB rotation shearing rates. In particular, the National Spherical Torus Experiment (NSTX) operates between 0.35 and 0.55 T, which, when coupled to up to 7 MW of neutral beam injection, leads to central rotation velocities in excess of 300 km/s. The Mach numbers of these central rotation velocities can be in excess of $M_s=0.5$ and range up to 0.85. ExB shearing rates reach 1 MHz, and this level of ExB shear can be up to a factor of five greater than typical linear growth rates of long-wavelength ion (e.g., ITG)

modes, suppressing these instabilities partially if not completely, and often leading to the development of ion Internal Transport Barriers in low density L-modes [8]. Further circumstantial evidence for this turbulence reduction is that the inferred diffusive ion thermal flux in typical NSTX H-modes is at or near the neoclassical level, and thus these plasmas operate in an electron-dominated transport regime. In fact, possibly because of the believed sub-dominance of the low-k turbulence, the energy confinement scalings in NSTX were found to differ from those at higher aspect ratio. In NSTX H-modes, the energy confinement time, τ_E , scales as $\sim B_T^{0.9} I_p^{0.4}$ (B_T is toroidal magnetic field and I_p is plasma current), with the strong B_T scaling controlled primarily by the variation of the electron transport in the gradient region ($r/a > 0.4$, where r is the local radius and a is the plasma minor radius), while the weak I_p scaling is dominated by the variation in the ion transport, which is essentially neoclassical in that region [2, 3], as determined by NCLASS [9] and the non-local GTC-NEO [10] codes.

This paper will cover two main topics: the effect of rotation and rotation shear on plasma energy confinement and local transport, and the study of momentum transport properties in both steady-state and by using perturbative techniques, augmenting previous work on NSTX on this topic [11]. It is found that there is a direct connection between the local rotation and/or rotation shear and the inferred local ion thermal diffusivity, with the ion thermal diffusivity changing in a fashion consistent with reduction of low-k turbulence by the rotation shear. This result directly establishes the important role played by rotation profiles in determining local transport, and indicates the need to understand the source of the momentum transport that leads to the establishment of the rotation profiles. Effective momentum diffusivity values determined by solving the steady-state momentum balance in the NSTX electron-dominated regime are found to have differences with those at higher aspect ratio, with $\chi_i \gg \chi_\phi^{\text{eff}}$, although the ion energy and momentum diffusivities generally scale with one another in the gradient region, similar to what is observed at higher aspect ratio. These effective diffusivities are found to be much greater than the momentum diffusivity determined by neoclassical analysis, even in plasma regimes where $\chi_i \sim \chi_{i,\text{neo}}$, suggesting that it is a source other than collisions that drives the momentum transport. In the determination of the effective diffusivity, all of the momentum transport, whether it be due to diffusion or convection, is assumed to be diffusive. Perturbation experiments, in some situations, allow for a separation of the diffusive and convective (or pinch) components of the transport. Indeed, perturbative experiments using neutral beam and applied $n=3$ magnetic field pulses to change the plasma rotation in the core and outer region respectively, indicate the existence of inward momentum pinches that are significant, up to 40 m/s, and that are consistent with predictions from theories based on a low-k turbulence drive. This means that the principal source of momentum transport could be due to residual low-k turbulence.

2. Effect of Rotation and Rotation Shear on Plasma Performance

NSTX is equipped with the means of applying low- n ($n=1$ to 3) magnetic fields to the plasma edge using a set of six coils situated on the midplane outside the vacuum vessel [6]. These applied fields can be used statically or dynamically to correct low- n error fields, and/or to feedback suppress low- n MHD mode activity including saturated or growing RWM modes. More recently, these coils have been used for Edge Localized Mode (ELM)-pacing experiments [12]. For this study, this set of coils has been used in an $n=3$ configuration to apply non-resonant magnetic perturbations (NRMP) to modify the plasma rotation and rotation shear. The region of greatest torque due to these fields, as inferred by local changes in plasma rotation, is observed to be near a major radius $R=1.3$ m, which is in agreement with calculations of the torque due to Neoclassical Toroidal Viscosity in the presence of these

applied perturbed fields [13]. By changing the rotation and rotation profile (gradient) locally, it is possible to study directly how important an effect these parameters have on both the global energy confinement and local heat transport properties of the plasma.

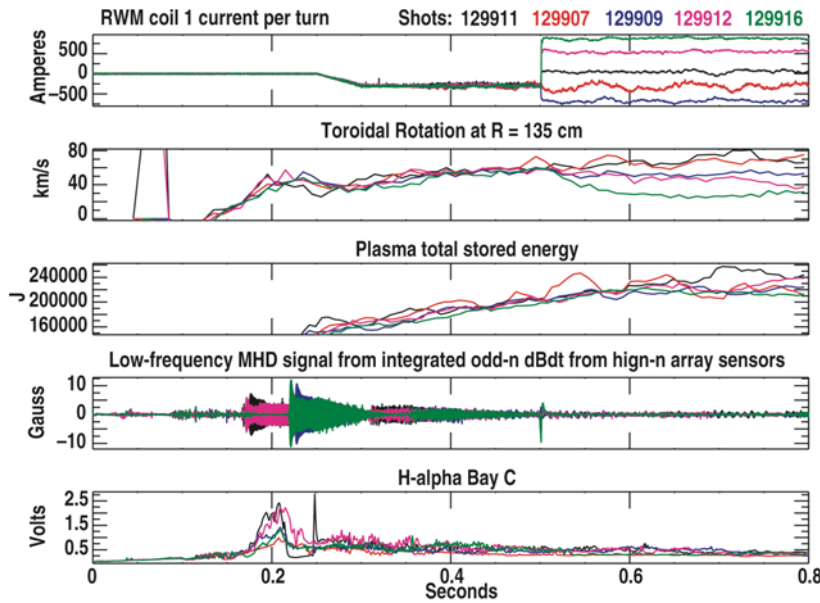


Fig. 1 Time traces for 5 H-mode discharges with application of different levels of $n=3$ braking fields. Shown from the top is the $n=3$ coil current, toroidal rotation at $R=1.35$ m, plasma stored energy calculated by the EFIT magnetic equilibrium reconstruction code, low-frequency MHD activity, and the D_α traces. The D_α emission reflects the edge plasma characteristics (e.g., n_e , T_e).

changed at $t=500$ ms; prior to that time, the current in the coils was optimized to correct the $n=3$ intrinsic error field and to feedback on low-frequency $n=1$ MHD modes. The plasma toroidal rotation in NSTX is measured by the charge exchange recombination spectroscopy (CHERS) diagnostic, which is based on measurement of the carbon impurity. NCLASS calculations indicate only a minor difference ($<5\%$) between the toroidal rotation of the carbon and that of the computed main ion species (D^+). The rotation at $R=1.35$ m is seen to change with the application of the $n=3$ fields (second panel from top), with each discharge reaching a new rotational equilibrium in this MHD- and ELM-free period (bottom two panels). The rotation ranges from 25 km/s to close to 80 km/s over the range of applied $n=3$ fields. The plasma stored energy (middle panel, note the suppressed zero in the ordinate) shows little variation with the different levels of plasma rotation.

In Fig. 2 is shown the stored energy of the plasma plotted as a function of plasma angular velocity, Ω (Fig. 2a) and angular velocity shear, $\nabla\Omega$ (Fig. 2b) for the discharges shown in Fig. 1 as well as other discharges in this experimental scan. Increasing shear is towards the left in the right panel of Fig. 2. Each figure shows the electron (red), ion (blue) and total stored energy (including fast ions) for the discharges in the scan, at a time of $t=0.72$ s, which is after the discharges have achieved rotation equilibrium. There appears to be only a slight, if any increase of stored energy in the thermal plasma species with either increasing rotation or rotation shear, although slightly more of an effect is seen in the total stored energy, where there is a comparable increase in fast ion to total plasma (electron + ion) stored energy. The energy contained in the rotation of the plasma ranges from only 1 to 4% (2 to 10 kJ) of the

The time evolution of a representative series of 4 MW neutral beam heated H-mode discharges for which the $n=3$ fields were applied at various strengths is shown in Fig. 1. These plasmas had $I_p=0.9$ MA and $B_T=0.45$ T, and they were run in the Lower Single Null configuration (dominant X-point in the lower part of the vessel) with an elongation of 2.4. The top panel of the figure shows the level of current in the NRMP coils for the $n=3$ configuration. 500 A/turn leads to a perturbation of the radial magnetic field, ΔB_r , of several Gauss in the plasma. The $n=3$ applied fields were

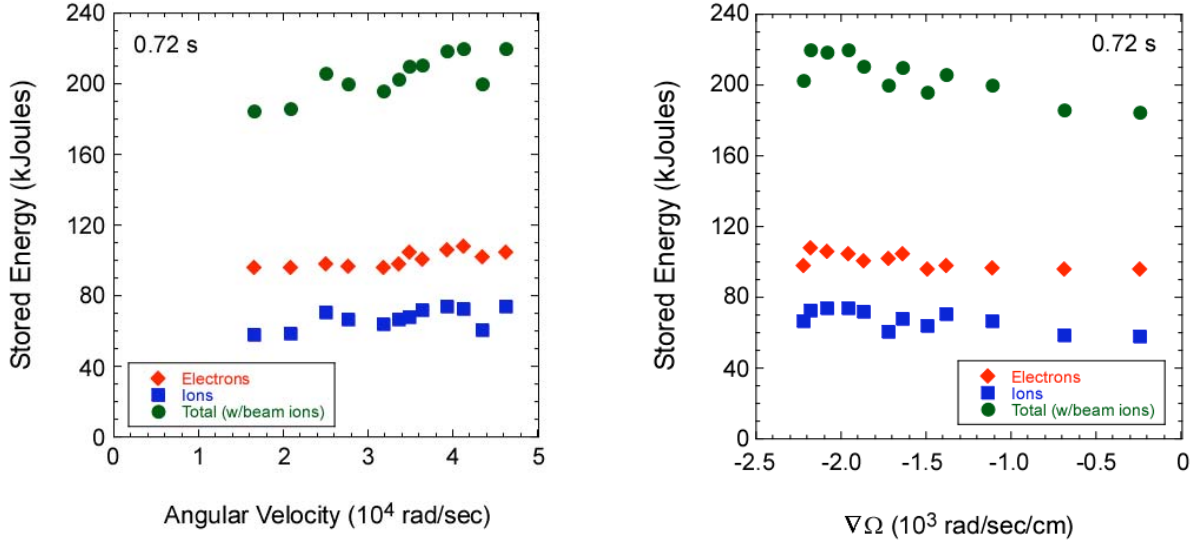


Fig. 2 Stored energy of ions, electrons, and total (including fast ions) as a function of Ω (left panel) and $\nabla\Omega$ (right panel). Ω and $\nabla\Omega$ are taken at $r/a \sim 0.75$.

total stored energy, and this variation constitutes only a minor contribution to the observed small increase of stored energy with rotation.

The change in rotation and rotation shear is found to be maximum, however, in just a limited spatial range of the plasma, which in these cases is the region from $r/a \sim 0.6$ to 0.9 . Consequently, it is not readily apparent that a change in these parameters in such a local region would affect the plasma on a global scale. Fig. 3 shows the rotation and rotation shear profiles (Fig. 3a and 3b respectively) for three representative discharges in which the applied braking was varied from zero (no braking), as indicated by the red curves to maximum

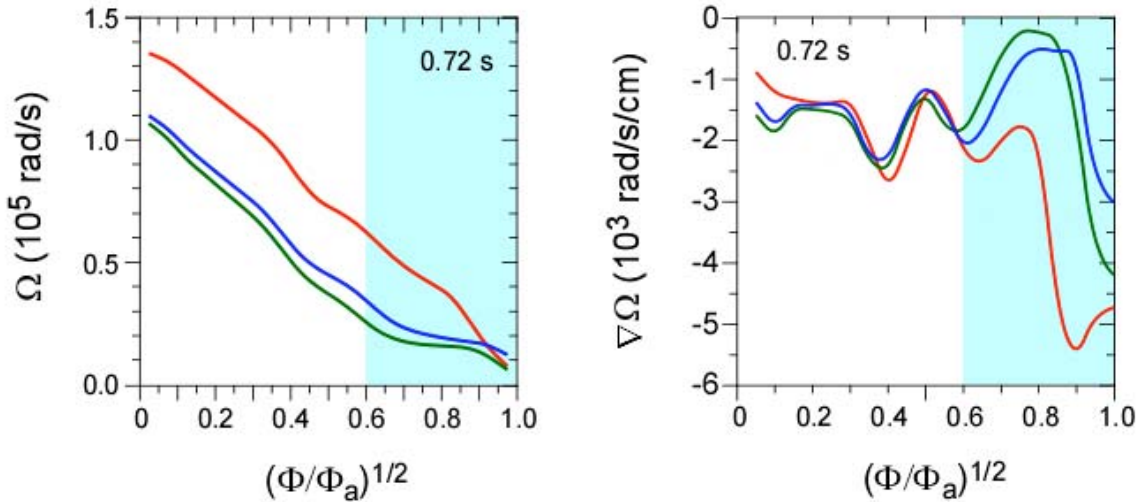


Fig. 3 Rotation (left panel) and rotation shear (right panel) as a function of the square root of local toroidal flux normalized to the value at the plasma boundary ($\propto r/a$) for three representative discharges in the applied $n=3$ field scan. The red curve is the discharge with no applied external field, while the green curve is the discharge with maximum applied field (braking). The angular rotation values in the blue shaded region are in the range from 2 to 4 times $v_{th,i}/R$.

braking, as indicated by the green curves. The rotation and rotation shear span the ranges from 2 to 6 x 10⁴ rad/s and -0.2 to -2.4 x 10³ rad/s/cm for the two respective cases for $(\Phi/\Phi_a)^{1/2} > 0.6$. The case with no applied braking (maximum rotation and rotation shear) is representative of the typical H-mode scenario in NSTX. Fig. 4 shows the ion (left panel) and electron (right panel) thermal diffusivities for these three representative discharges. The thermal diffusivity values in the region near $r/a=0.75$ to 0.85 show a clear reduction with increasing Ω and $\nabla\Omega$. This is particularly true in the ion channel, where there is a factor of almost three difference between the maximum and minimum Ω and $\nabla\Omega$ cases. For the ions, the ratio of $\chi_i/\chi_{i,neo}$ increases from 1.2 (for the typical H-mode case) to 3.9 with decreasing Ω and $\nabla\Omega$. The variation in core χ_i is due to a variation in the central ion heating power.

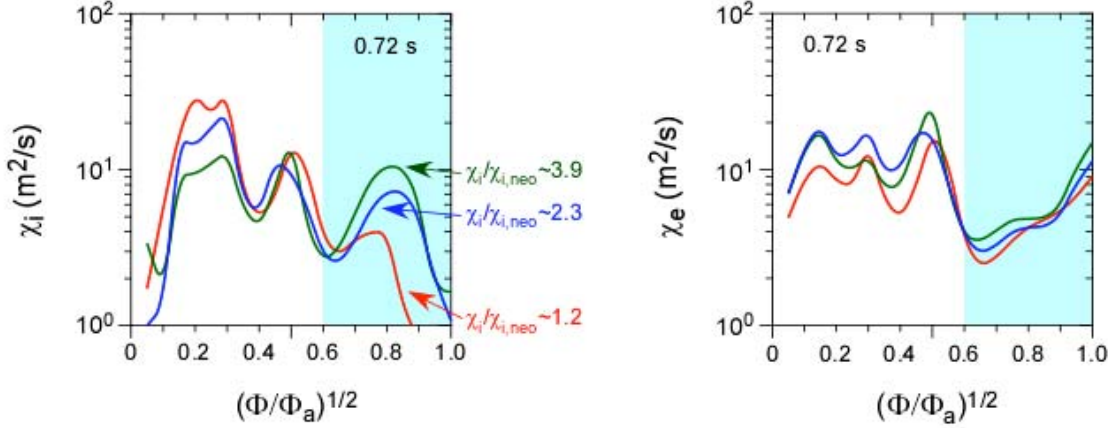


Fig. 4 Ion thermal diffusivity (left panel) and electron thermal diffusivity (right panel) for the discharges in the applied $n=3$ field scan shown in Fig. 3. Also shown are the ratios of ion thermal diffusivity to the neoclassical value for the three discharges.

This dependence of χ_i on $\nabla\Omega$ can be understood in terms of the degree of suppression of low- k turbulence by rotation (ExB) shear. Fig. 5 shows results from linear GS2 [14, 15] gyrokinetic calculations of the growth rates of low- k turbulence in the minimum and maximum Ω and $\nabla\Omega$ cases. While the linear growth rates for the two cases are similar (solid curves), indicating that the general characteristics of the two plasmas are similar (e.g., T_e , n_e , T_i , n_D , q , etc), the ExB shearing rates are not, with the maximum Ω and $\nabla\Omega$ case having ω_{ExB} a factor of five higher than the linear growth rate (red), and the minimum case (green) having the two rates comparable. This result suggests more of a reduction in the low- k (ITG/TEM) turbulence in one case than the other, and it is consistent with the increase $\chi_i/\chi_{i,neo}$ from ~ 1 to ~ 4 going from the case with $\omega_{ExB} \gg \gamma_{lin}$ (typical H-mode) to the one with $\omega_{ExB} \sim \gamma_{lin}$. It should be noted that the GS2 growth rate calculation does not include the measured high toroidal rotation rates, which is potentially a source of uncertainty in these theoretical results. It should be noted further that calculations using IPEC to determine the plasma response to applied magnetic perturbations [16] indicate a lack of stochasticity in the outer region of the discharge

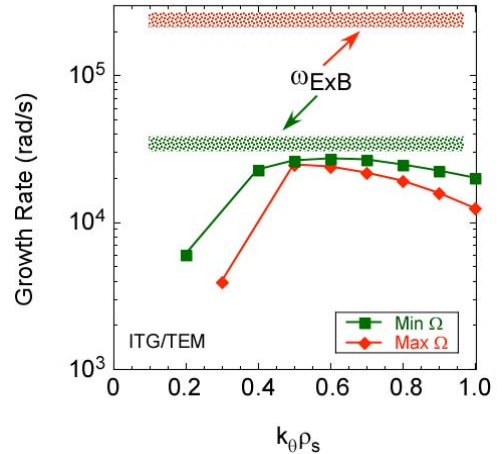


Fig. 5 Linear growth rates from GS2 along with ExB shearing rates for the two extreme discharges.

due to plasma shielding effects of the applied $n=3$ fields. This result supports the conclusion that the change in ion thermal diffusivity is related to the magnitude of ω_{ExB} and its effect on low- k turbulence.

3. Momentum Transport Studies

The results in Section 1 showed the importance of the ExB shear in controlling transport locally, and that with sufficient rotation shear the ion transport is near neoclassical and the transport loss is dominated by the anomalous electrons. In this section the source of momentum transport is studied using both steady-state and perturbative techniques.

Values of χ_i and χ_ϕ^{eff} from TRANSP [17, 18] steady-state analysis for $r/a \sim 0.4$ (left panel) and 0.65 (right panel) in both L- and H-modes are plotted versus one another in Fig. 6. The neutral beams are assumed to be the only source of torque in the steady-state analysis, in which the momentum pinch is assumed implicitly to be zero. The figure shows that $\chi_i > \chi_\phi^{\text{eff}}$ by as much as over an order of magnitude at both locations, although there does appear to be a statistical

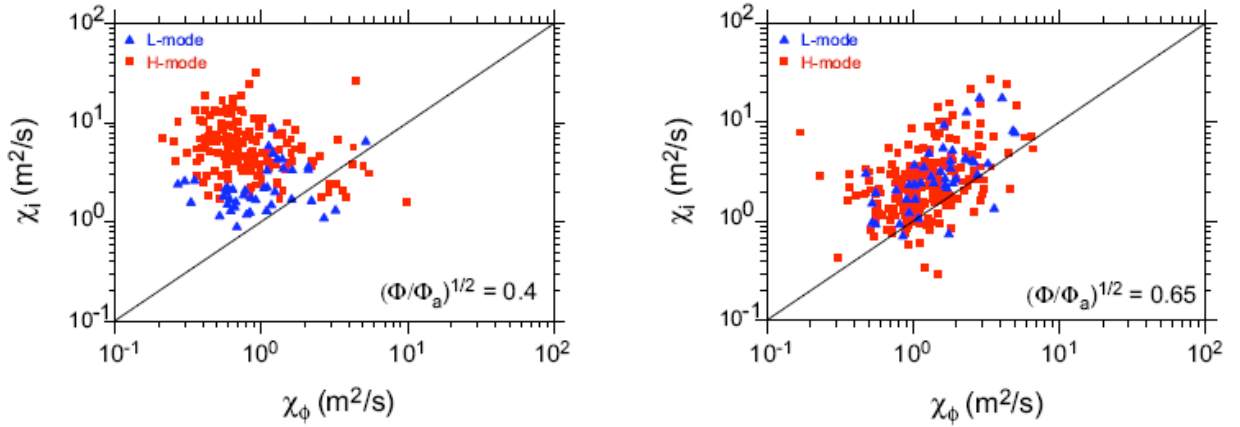


Fig. 6 χ_i vs χ_ϕ^{eff} as determined from steady-state analysis for $r/a \sim 0.4$ (left panel) and $r/a \sim 0.65$ (right panel)

coupling between χ_i and χ_ϕ^{eff} at $r/a=0.65$, qualitatively consistent with results from higher aspect ratio tokamaks [19, 20]. For the NSTX points at this outer radius, the average Prandtl number range, $\chi_\phi^{\text{eff}}/\chi_i$, is 0.2-0.5. There is no statistical coupling between χ_e and χ_ϕ^{eff} at any radius, with $\chi_e \gg \chi_\phi^{\text{eff}}$.

Because of the coupling between χ_i and χ_ϕ^{eff} in this region of the plasma, where χ_i can often be close to neoclassical, it is natural to explore whether χ_ϕ^{eff} is also controlled by neoclassical processes. GTC-NEO, which self-consistently includes the measured toroidal rotation profiles, has been used to address this, with the results for H-modes shown in Fig. 7. Plotted in this figure are the experimentally inferred χ_i and χ_ϕ^{eff} (solid blue and red lines respectively) along with the values determined from GTC-NEO (dashed blue and red lines). For the H-mode discharge (left panel), it can be seen that while the experimentally inferred χ_i is essentially at the neoclassical level across the plasma, $\chi_\phi \gg \chi_{\phi,\text{neo}}$, which is essentially zero. This result is robust, even when $\chi_i/\chi_{i,\text{neo}} > 1$, as in high density L-mode plasmas (right panel). This result indicates, then, that the primary driver for the momentum transport must be

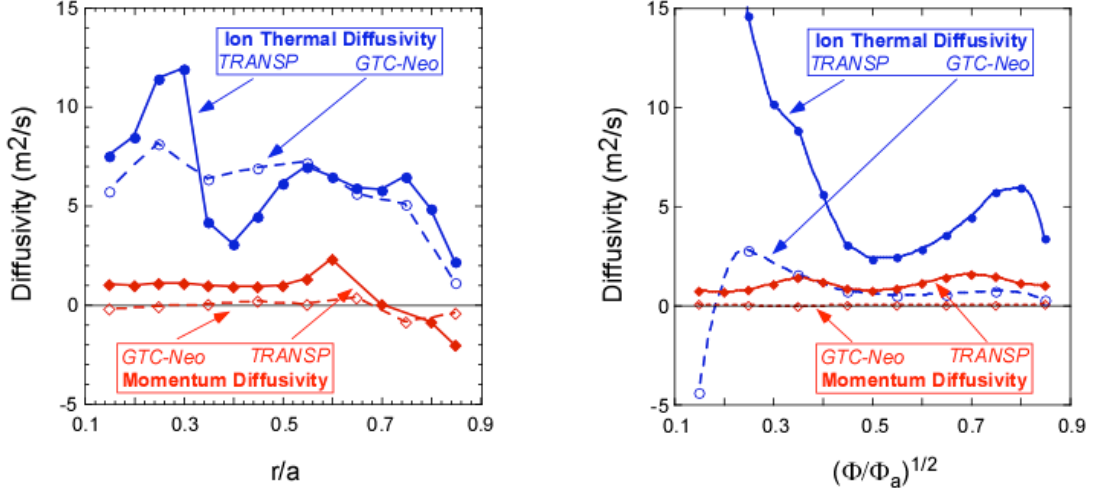


Fig. 7 Experimentally inferred values of χ_i and χ_ϕ compared to the neoclassical values computed by GTC-NEO for an H-mode (left panel) and an L-mode (right panel) plasma.

something other than collisional (neoclassical) processes. It is worthwhile to note that $\chi_{i,neo}$ is relatively large, and at least as large as χ_ϕ .

To explore other possible sources of momentum transport, perturbation experiments, which can yield both the momentum diffusivity and any possible momentum pinch, are important. To determine the momentum diffusivity and pinch, torque perturbations were applied using either 200 ms neutral beam pulses of approximately 4 MW (in addition to steady 2 MW injection), which changed rotation primarily in the core, or 50 ms pulses of $n=3$ braking fields, which changed the rotation primarily in the outer (gradient) region. In the first scenario, the rotation in the core responded immediately in response to a factor of two to three increase in NB torque for $r/a < 0.25$, similar to the response shown in Fig. 1. In the latter scenario, the rotation near $R=1.35$ m responded immediately, with a delayed and much more gradual change seen in the core. Using the measured angular velocity profiles and a determination of the neutral beam torque, the angular momentum balance was calculated in TRANSP. For the pulsed NB cases, the chosen time of analysis began with the NBI pulse, while for the application of the $n=3$ braking fields, the time of analysis began immediately after the braking pulse was turned off. This period was chosen in the latter scenario since the NB induced torque, the only known torque at that time, is more readily calculated than that from the applied $n=3$ fields [11].

The momentum flux, Γ_ϕ , including both a diffusion and a pinch term, can be written

$$\Gamma_\phi = -mnR\chi_\phi \frac{\partial v_\phi}{\partial r} + mnRv_{pinch}v_\phi$$

where v_ϕ is the measured toroidal velocity and Γ_ϕ is calculated in TRANSP. χ_ϕ and v_{pinch} are modelled by assuming they are constant in time during the analysis period, and solving the above equation using a nonlinear least squares fit [for details see Ref. 11]. In order to determine both χ_ϕ and v_{pinch} independently, the changes in v_ϕ and ∇v_ϕ in response to the change in torque have to be decoupled. This requirement was satisfied in the outer region of the plasma for the $n=3$ field pulses, but only for a limited spatial region in the core for the NBI pulses.

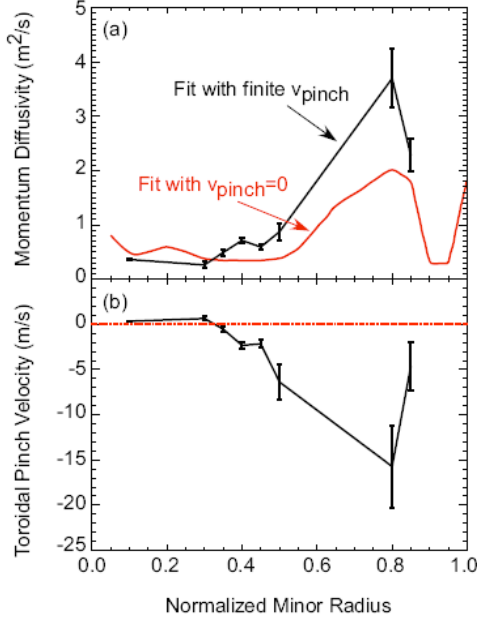


Fig. 8 (a) momentum diffusivity and (b) pinch velocity inferred using $n=3$ magnetic braking. The inferred diffusivity assuming $v_{pinch}=0$ is shown in red.

turbulence in the plasma, Peeters et al. [21] and Hahm et al. [22]. Both theories find that $v_{pinch} \sim \chi_\phi / R$, although Peeters claims an additional dependence on the density gradient scale length, L_n . A comparison of v_{pinch} as computed by these theories to the experimentally inferred values for the outer region of the plasma is shown in Fig. 9. The red points in the figure show the v_{pinch} computed by the Hahm theory, while the blue points show those computed with the Peeters theory, both sets as functions of the experimentally inferred pinch velocities. The best fits through the data (forcing the fit through zero) is shown by the color-coded lines and fit equations in the figure. In general, both theories indicate reasonable agreement with the inferred values, although the Peeters theory, while exhibiting a higher degree of scatter, appears to fit better especially for larger v_{pinch} . This is seen by the fact that the best fit through the Peeters points have a slope of ~ 1.1 , as compared to 0.64 for the Hahm points. The better fit by the Peeters theory is due to the presence of the L_n term. The larger v_{pinch} (>20 m/s) typically occur for lower L_n (~ 0.1 to 0.2 m), and it is in this range where Peeters does a better job fitting the experimental points. Both theories do equally well for lower v_{pinch} , where $L_n=0.2$ to 1 m. In the inner region, the comparison between the inferred pinch velocities and those calculated by either theory was poor for all L_n as is seen in Fig. 10. The experimentally inferred values of v_{pinch} were small, ≤ 10 m/s, while the predicted values could be much larger, up to 25 m/s. These results are consistent with linear gyrokinetic calculations indicating that ITG/TEM modes are unstable in the outer region, where the experimental and predicted pinch velocities generally agree, but stable in the core in these plasmas, where the two do not agree.

The results for one such case, in the outer portion of the plasma, is shown in Fig. 8. The momentum diffusivity is shown for a case with finite v_{pinch} , and for the case where v_{pinch} is assumed to be zero in solving the above equation. It can be seen that the χ_ϕ with non-zero v_{pinch} can be several times larger than that when v_{pinch} is assumed to be zero. This would mean that the large ratio of χ_i/χ_ϕ shown in Fig. 7 would trend lower when a pinch term is included in the analysis. Furthermore, the inward pinch can be significant (bottom panel), in this case with a value of up to 20 m/s, with corresponding $\chi_\phi \sim 3.5$ m²/s, in the region from $r/a=0.6$ to 0.8 . Other cases show v_{pinch} up to 40 m/s, also with corresponding χ_ϕ values up to 4 m²/s. I_p and B_T scans revealed a decrease in χ_ϕ with B_T in the outer region of the plasma, but little dependence of χ_ϕ or v_{pinch} with plasma current. No dependences were observed in the core region.

There have been two theories suggesting that the source of the momentum pinch is low-k

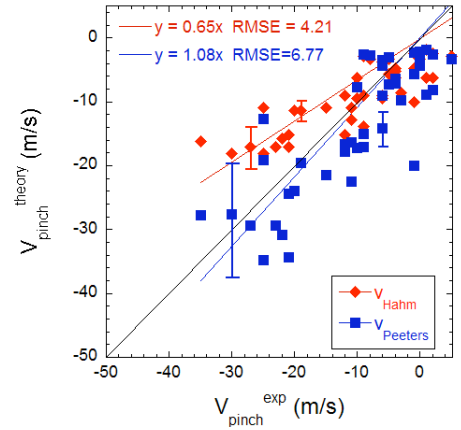


Fig. 9 V_{pinch} as computed by the Hahm (red) and Peeters (blue) theories vs experimentally inferred values for the outer region of the plasma.

4. Summary and Discussion

The application of $n=3$ non-resonant magnetic perturbations to modify the plasma rotation was shown to change not only the rotation locally in the region of maximum torque ($R \sim 1.3$ m), but also to change the rotational shear. Because the torque perturbation is limited spatially, the effect on the overall stored energy of the plasma is small. However, the modification in rotation shear is seen to affect the local χ_i ; there is an obvious increase in χ_i and $\chi_i/\chi_{i,neo}$, the latter from values of ~ 1 with no magnetic braking (e.g., the typical H-mode scenario in NSTX) to values ~ 4 with maximum braking and lower rotational shear. This trend is consistent with decreasing suppression of low- k turbulence with decreasing ExB shear. As the shear decreases to values near the linear growth rate of the ITG/TEM modes, the ion thermal diffusivity becomes more anomalous. For $\omega_{ExB} \gg \gamma_{lin}$, the ion transport is near neoclassical, due to at least partial suppression of these low- k modes.

The steady-state momentum diffusivity can be over an order of magnitude greater than χ_i , but the ratio χ_i/χ_ϕ trends closer to 1 (but still remains a factor of several), when an inward pinch, which can be significant, is taken into account. The Prandtl number ranges from 0.2 to 0.5 for steady-state values of χ_ϕ , but increases to 0.5 to 0.8 when the pinch term is taken into account, consistent with results from gyrokinetic calculations [23]. The magnitude of the inward pinch in the outer region is consistent with values determined from theories based on low- k turbulence, while the agreement is poor in the core, consistent with results from linear gyrokinetic calculations indicating that ITG/TEM modes are unstable in the outer region but stable in the core. The data-theory comparison shows the importance of including a $1/L_n$ term. That the momentum pinch in the outer region is in general agreement with a low- k turbulence drive holds irrespective of whether the ion energy transport is neoclassical, which is the case for most H-mode plasmas, or not. This result is due to the fact that the ion neoclassical energy transport is large, and thus can dominate the low- k turbulence induced transport that is effectively reduced by large ExB shear. The neoclassical momentum diffusivity, however, is essentially zero, and thus is subdominant to whatever low- k turbulence induced transport remains after being reduced by ExB shear. Therefore, the momentum transport in the electron-dominated plasmas of NSTX can be a better probe of the low- k turbulence than ion energy transport. A Beam Emission Spectroscopy system that will measure the turbulence spectrum at low- k is presently being installed on NSTX, and future experiments will be performed to investigate the relation of the low- k turbulence and momentum and heat transport.

We thank J.K. Park for the IPEC calculations. This work was supported by U.S. DOE Contract No. DE-AC02-76CH03073 at the Princeton Plasma Physics Laboratory, and No. DE-FG02-99ER54523 at Columbia University.

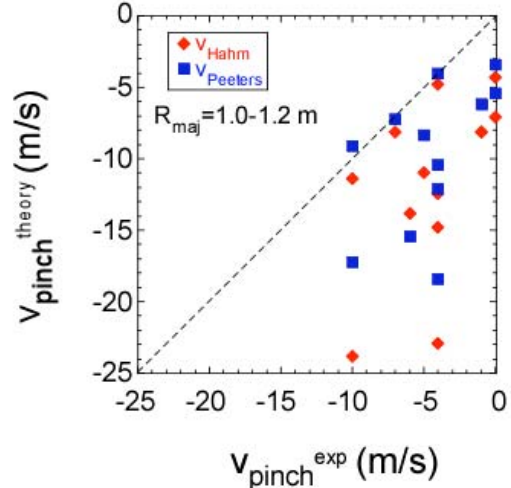


Fig. 10 V_{pinch} as computed by the Hahm (red) and Peeters (blue) theories vs experimentally inferred values for the inner region of the plasma.

References

- [1] BURRELL, K., Phys. Plasmas **4** (1997) 1499.
- [2] KAYE, S.M., Phys. Rev. Lett. **98** (2007) 175002.
- [3] KAYE, S.M. et al., Nuc. Fusion **47** (2007) 499.
- [4] SMITH, D.R., Phys. Rev. Lett., in preparation (2008).
- [5] MENARD, J.E. et al., Nuc. Fusion **45** (2005) 539.
- [6] STRAIT, E.J., et al. Phys. Rev Lett. **74** (1995) 2483.
- [7] SABBAGH, S.A. et al., Phys. Rev. Lett. **97** (2006) 045004.
- [8] YUH, H., et al., Phys. Rev. Lett., in preparation (2008).
- [9] HOULBERG, et al., Phys. Plasmas **4** (1997) 3230.
- [10] WANG, W. et al., Comput. Phys. Commun., **164** (2004) 178.
- [11] SOLOMON, W.A., et al., Phys. Rev. Lett. **101** (2008) 065004.
- [12] CANIK, J., in Fusion Energy 2008 (Proc. 22nd Int. Conf. Geneva, 2008) (Vienna: IAEA) CD-ROM file PD/P1-5 and <http://www-naweb.iaea.org/napc/physics/FEC/FEC2008/html/index.htm>
- [13] ZHU, W., et al., Phys. Rev. Lett. **96** (2006) 225002.
- [14] KOTSCHENREUTHER, M., et al., Comput. Phys. Commun., **88** (1995) 128.
- [15] DORLAND, W. et al., Phys. Rev. Lett. **85** (2000) 5579.
- [16] PARK, J.K. et al., Phys. Rev. Lett. **99** (2007) 195003.
- [17] HAWRLUK, R., in Physics of Plasmas Close to Thermonuclear Conditions (Proc. Course Varenna 1979) Vol. 1, Commission of the European Communities, Brussels (1979) 19.
- [18] GOLDSTON, R.J., et al., J. Comput. Phys. **43** (1981) 61.
- [19] NISHIJIMA, D. et al., Plasma Phys. Contr. Fusion **47** (2005) 89.
- [20] deVRIES, P.C., et al., Plasma Phys. Controlled Fusion **48** (2006) 1693.
- [21] PEETERS, A., C. ANGIONI and D. STRINTZI, Phys. Rev. Lett. **98** (2007) 265003.
- [22] HAHM, T.S., et al., Phys. Plasmas **14** (2007) 072302.
- [22] PEETERS, A.G. and C. ANGIONI, Phys. Plasmas **12** (2005) 072515.

The Princeton Plasma Physics Laboratory is operated
by Princeton University under contract
with the U.S. Department of Energy.

Information Services
Princeton Plasma Physics Laboratory
P.O. Box 451
Princeton, NJ 08543

Phone: 609-243-2750
Fax: 609-243-2751
e-mail: pppl_info@pppl.gov
Internet Address: <http://www.pppl.gov>